J. Fluid Mech. (2020), *vol*. 904, A4.
Published by Cambridge University Press

doi:10.1017/jfm.2020.647

Solitary waves on constant vorticity flows with an interior stagnation point

V. Kozlov[1], **N. Kuznetsov**[2] **and E. Lokharu**[1,†]

[1]Department of Mathematics, Linköping University, S-581 83 Linköping, Sweden

[2]Laboratory for Mathematical Modelling of Wave Phenomena, Institute for Problems in Mechanical Engineering, Russian Academy of Sciences, VO, Bol'shoy pr. 61, St Petersburg 199178, Russian Federation

(Received 10 January 2020; revised 13 July 2020; accepted 28 July 2020)

The two-dimensional free-boundary problem describing steady gravity waves with vorticity on water of finite depth is considered. Under the assumption that the vorticity is a negative constant whose absolute value is sufficiently large, we construct a solution with the following properties. The corresponding flow is unidirectional at infinity and has a solitary wave of elevation as its upper boundary; under this unidirectional flow, there is a bounded domain adjacent to the bottom, which surrounds an interior stagnation point and is divided into two subdomains with opposite directions of flow by a critical level curve connecting two stagnation points on the bottom.

Key words: solitary waves, critical layers, surface gravity waves

1. Introduction

In the present paper, we consider the problem describing two-dimensional gravity waves travelling on a flow of finite depth. For an ideal fluid of constant density, say water, the effects of surface tension are neglected, whereas the flow is assumed to be rotational with a constant vorticity; this, according to observations, is a type of motion commonly occurring in nature (see, for example, Swan, Cummings & James (2001), Thomas (1981) and references therein). Also, it is assumed that the reference frame is moving with the wave so that the relative velocity field is stationary. Our aim is to consider a new class of solitary waves each having a cat's-eye – a region of closed streamlines surrounding a stagnation point. To the best of the authors' knowledge, there are no results concerning solitary waves having such a pattern of streamlines; so far, this kind of behaviour has been known only for periodic waves with vorticity.

The mathematical theory of two-dimensional solitary waves on irrotational flows goes back to the discovery of John Scott Russell, who was the first to observe in 1834 and subsequently to analyse a solitary wave of elevation (see Russell 1844). The existence of the latter was justified mathematically by Boussinesq in 1877 and rediscovered by Korteweg and de Vries in 1895. The existence of solitary waves in the framework of the full

† Email address for correspondence: evgeniy.lokharu@liu.se

water wave problem is far more complicated and the first proofs were obtained much later (Lavrentiev 1954; Friedrichs & Hyers 1954). Modern proofs by Thomas (1977) and Mielke (1988) use the Nash–Moser implicit function theorem and a dynamical system approach, respectively. All these papers deal only with waves of small amplitude, whereas Amick & Toland (1981*b*) constructed large-amplitude solitary waves using global bifurcation theory and then proved the existence of a limiting wave of the extreme form, that is, having an angled crest (see Amick, Fraenkel & Toland 1982). All solitary waves considered in these papers are of positive elevation, symmetric and monotone on each side of the crest (see Craig & Sternberg 1988; McLeod 1984). The corresponding flows, being irrotatonal, have a simple structure of streamlines (see Constantin & Escher 2007; Constantin 2010): they are unbounded curves similar (diffeomorphic) to the free surface profile. For all unidirectional waves with vorticity (when the horizontal component u of the relative velocity field has a constant sign everywhere in the fluid), the latter property is also true. Essentially, this forbids the presence of critical layers and stagnation points.

The first construction of unidirectional small-amplitude solitary waves with vorticity was given by Ter-Krikorov (1962), whereas Benjamin (1962) obtained an approximate form of the wave profile which is the same as in the irrotational case. However, relationships between the wave amplitude, the length scale and the propagation velocities depend on the primary velocity distribution in a complicated way. Much later, Groves & Wahlén (2008) and Hur (2008) obtained new results for this topic. The latter authors also considered solitary waves with vorticity in the presence of surface tension (Groves & Wahlén 2007). The method used in Groves & Wahlén (2007, 2008), known as spatial dynamics, is essentially an infinite-dimensional version of the centre-manifold reduction which is known as spatial dynamics because it is applied to a Hamiltonian system with the horizontal spatial coordinate playing the role of time. The first use of this method in the water-wave theory is due to Kirchgässner (1982, 1988) (see also Mielke 1986, 1988, 1991), whereas an application of spatial dynamics to three-dimensional waves is given in Groves & Nilsson (2018) (see also references therein). So far, use of spatial dynamics has been restricted exclusively to small-amplitude waves. Recently, Wheeler (2013) examined waves of large amplitude, but, like in the irrotational case, all solitary-wave solutions have the same structure of streamlines, that is, are symmetric and of positive elevation (see Hur 2008; Wheeler 2015; Kozlov, Kuznetsov & Lokharu 2015, 2017). Thus, looking for a more complicated geometry of solitary waves, it is natural to consider flows with stagnation points and critical levels within the fluid domain. As in Wahlén (2009), by a critical level we mean a curve for which the horizontal component of velocity vanishes.

The simplest case of flows with critical levels is that of constant negative vorticity, and there are several advantages of studying this case. Flows with constant vorticity are more easily tractable mathematically (see Ehrnström 2008; Wahlén 2009; Constantin, Strauss & Vărvărucă 2016; Hur & Wheeler 2020). Moreover, these flows are of substantial practical importance being pertinent to a wide range of hydrodynamic phenomena (see Constantin *et al.* 2016, p. 196); an important example are currents producing shear near the sea bed. A new feature of laminar flows with constant vorticity (compared with irrotational ones) is that there are flows with critical levels. Moreover, it was shown by Wahlén (2009) that small perturbations of these parallel flows are periodic waves with arrays of cat's-eye vortices – regions where closed streamlines surround stagnation points. An extension to periodic waves of large amplitude with critical layers is given in Constantin *et al.* (2016) (it includes overhanging waves). Despite the fact that waves considered in Wahlén (2009) and Constantin *et al.* (2016) have critical layers, the geometry of free-surface profiles is still simple; it is symmetric about every crest and trough, whereas monotone in between

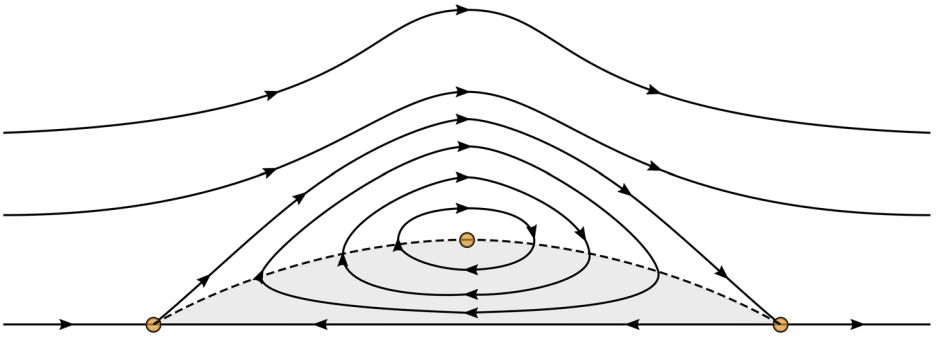

FIGURE 1. A sketch of a streamline pattern. Solid lines are streamlines and the direction of the flow (in the moving frame) is denoted by arrows. The dashed curve is a critical layer, where the horizontal component of the velocity field vanishes, while circles are stagnation points. The direction of the flow below the critical layer (grey region) is opposite to the direction of the flow above it.

(just like that of the classical Stokes waves). Examples of more complicated wave profiles are known (see Ehrnström, Escher & Wahlén 2011; Aasen & Varholm 2017; Kozlov & Lokharu 2017, 2019). However, the vorticity distribution must be at least linear in order to construct them. It should be emphasized that all theoretical studies of waves with critical layers have been restricted so far to the periodic setting.

In the 1980s and 1990s, much attention was devoted to numerical computation of various solitary waves on flows with constant vorticity; see the papers by Vanden-Broeck (1994, 1995) and references therein. In particular, an interesting family of solitary-wave profiles was obtained in the second of these papers; it approaches a singular one with trapped circular bulb at the crest which happens as the gravity acceleration tends to zero. However, no attempt was made to find bottom or interior stagnation points for solitary waves. On the other hand, Teles da Silva & Peregrine (1988) were the first who numerically observed eddies surrounding interior stagnation points beneath wave crests of periodic waves on water of finite depth with constant vorticity (see also Ribeiro, Milewski & Nachbin 2017).

In the present paper, a new family of solitary waves is constructed for large negative values of the constant vorticity. All these waves have a remarkable property: the corresponding flow is unidirectional at both infinities, but there is a cat's-eye vortex centred below the wave crest (see figure 1). (The term was coined by Kelvin in his considerations of a shear flow having this pattern of streamlines; see Majda & Bertozzi 2002, pp. 53–54.) The vortex is bottom-adjacent and separated from the unidirectional flow above it by a critical streamline connecting two stagnation points on the bottom. Every solitary wave under consideration is obtained as a long-wave limit of Stokes wave-trains; in this aspect, our result is similar to that of Amick & Toland (1981*a*), who dealt with the irrotational case. However, Stokes waves have a cat's-eye vortex centred below each crest in our case. For a sketch of the corresponding streamline pattern, see the top part of figure 4, whereas examples computed numerically are presented in Ribeiro *et al.* (2017, pp. 803–804). As the wavelength goes to infinity, these vortices do not shrink, which differs from the case of small-amplitude waves, a sketch of which is plotted by Wahlén (2009) in his figure 1. A sketch of streamlines corresponding to our solitary wave is plotted in figure 1, where the circles denote stagnation points. Moreover, the dashed line shows the critical level along which the horizontal component of velocity vanishes and the critical

streamline located above the critical level also connects the two bottom stagnation points; the direction of streaming is indicated by arrows.

It should be emphasized that small-amplitude solitary waves constructed in this paper cannot be captured by applying spatial dynamics directly because the problem turns, in some sense, into a singular one as the vorticity tends to infinity. Thus, an appropriate scaling and a careful analysis are required before spatial dynamics can be used.

The plan of the paper is as follows. Statement of the problem and formulation of the main results are given in § 1.1. Then, in § 2, the problem is scaled and reformulated in a suitable way. After that, in § 3, it is reduced to a finite-dimensional Hamiltonian system and theorem 3.2 provides the existence of solitary waves. Then the main theorem 1.1 is proved in § 4. A discussion of the presented results is given in § 5.

1.1. *Statement of the problem and formulation of the main result*

Let an open channel of uniform rectangular cross-section be bounded from below by a horizontal rigid bottom and let water occupying the channel be bounded from above by a free surface not touching the bottom. The surface tension is neglected and the pressure is assumed to be constant on the free surface. In appropriate Cartesian coordinates (X, Y), the bottom coincides with the X axis and gravity acts in the negative Y direction. The frame of reference is chosen so that the velocity field is time-independent as well as the unknown free-surface profile. The latter is assumed to be the graph of $Y = \eta(X)$, $X \in \mathbb{R}$, where η is a positive function; we note that for irrotational waves this is always true (see Varvaruca 2008). The water motion is supposed to be two-dimensional and rotational, where the vorticity distribution is a constant; combining this and the incompressibility of water, we seek the velocity field in the form $(\psi_Y, -\psi_X)$, in which case $\psi(X, Y)$ is referred to as the stream function.

It is convenient to use the non-dimensional variables proposed by Keady & Norbury (1978). Namely, lengths and velocities are scaled to $(Q^2/g)^{1/3}$ and $(Qg)^{1/3}$, respectively, where Q is the mass flux and g is the acceleration due to gravity. Thus, Q and g are equal to unity in this case. Since the surface tension is neglected, the pair (ψ, η) must satisfy the following free-boundary problem:

$$\psi_{XX} + \psi_{YY} - b = 0 \quad \text{for } 0 < Y < \eta(X), \tag{1.1a}$$

$$\psi(X, Y) = 0 \quad \text{on } Y = 0, \tag{1.1b}$$

$$\psi(X, Y) = 1 \quad \text{on } Y = \eta, \tag{1.1c}$$

$$|\nabla\psi(X, Y)|^2 + 2Y = R \quad \text{on } Y = \eta(X). \tag{1.1d}$$

Here $b > 0$ is the vorticity constant, while constant R is considered as a parameter of the problem; it is referred to as the total head or the Bernoulli constant (e.g. Keady & Norbury 1978). This statement (with a general vorticity distribution) has long been known and its derivation from the governing equations and the assumptions about the boundary behaviour of water particles can be found in Constantin & Strauss (2004).

A solution of problem (1.1*a*)–(1.1*d*) defines a solitary wave provided the following relations hold:

$$\eta(X) \to h \quad \text{and} \quad |\psi_X(X, Y)| \to 0 \text{ as } X \to \pm\infty. \tag{1.2}$$

Here h is a constant, which coincides with the depth of a certain laminar flow at infinity. A sketch of the profile, which is typical for a solitary wave, is shown in figure 2. It should be noted that the flow at infinity is not uniform as it is in the irrotational case.

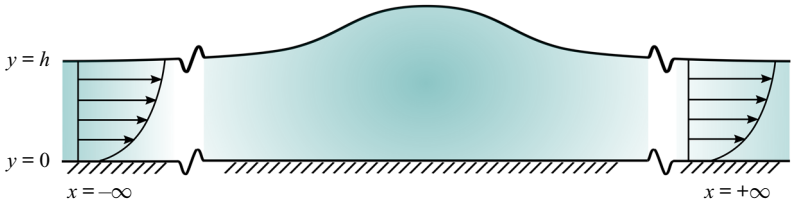

FIGURE 2. A sketch of the solitary wave profile on a unidirectional flow.

Now we are in a position to formulate our main result concerning the existence of solitary waves of elevation.

THEOREM 1.1. *For every sufficiently large $b > 0$, problem (1.1a)–(1.1d), (1.2) has a solution (ψ, η) with the following properties:*

(i) $\eta(X) > h$ *for all* $X \in \mathbb{R}$*, that is,* η *describes a solitary wave of elevation;*
(ii) there are two stagnation points on the bottom and two streamlines within the fluid domain connect these points (see figure 1); the critical level corresponds to the upper streamline, whereas the other one is on the bottom;
(iii) the critical streamline surrounds a region of streamlines around an interior stagnation point on the vertical line through the crest;
(iv) all streamlines above the critical one are diffeomorphic to the free-surface profile.

An equivalent formulation of this assertion and its proof are given in the next two sections. Our approach is based on a carefully chosen scaling of the original problem. Then we apply the spatial dynamics method to the scaled problem in the same way as in Kozlov & Lokharu (2019). This allows us to reduce the problem to a finite-dimensional Hamiltonian system; it has one degree of freedom and admits a homoclinic orbit describing a solitary wave of elevation in the original coordinates. The orbit goes around an equilibrium point representing a shear flow of constant depth with a counter-current and this guarantees the presence of a stagnation point and a critical streamline as is illustrated in figure 1.

2. Reformulation of the problem

To avoid difficulties arising from the fact that b is large, it is convenient to scale variables as follows:

$$\bar{x} = \sqrt{b}X, \quad \bar{y} = \sqrt{b}Y, \quad \bar{\eta}(\bar{x}) = \sqrt{b}\,\eta(X), \quad \bar{\psi}(\bar{x}, \bar{y}) = \psi(X, Y). \tag{2.1a–d}$$

This transforms (1.1a)–(1.1d) into

$$\bar{\psi}_{\bar{x}\bar{x}} + \bar{\psi}_{\bar{y}\bar{y}} - 1 = 0 \quad \text{for } 0 < \bar{y} < \bar{\eta}(\bar{x}), \tag{2.2a}$$

$$\bar{\psi}(\bar{x}, \bar{y}) = 0 \quad \text{on } \bar{y} = 0, \tag{2.2b}$$

$$\bar{\psi}(\bar{x}, \bar{y}) = 1 \quad \text{on } \bar{y} = \bar{\eta}, \tag{2.2c}$$

$$|\nabla\bar{\psi}|^2 + 2\gamma\bar{y} = \bar{R} \quad \text{on } \bar{y} = \bar{\eta}, \tag{2.2d}$$

where $\gamma = b^{-3/2}$ and $\bar{R} = Rb^{-1}$. This problem describes two-dimensional waves with vorticity (the latter is equal to one) and weak gravity because γ is a small parameter provided b is large.

Let us consider the stream solution $\bar{\psi} = u(\bar{y}; s)$ and $\bar{\eta} = h(s)$ such that $u'(0) = s$. From (2.2*a*)–(2.2*c*) one obtains the unique pair

$$u(\bar{y}; s) = \tfrac{1}{2}\bar{y}^2 + s\bar{y}, \quad h(s) = -s + \sqrt{2 + s^2}, \tag{2.3a,b}$$

and (2.2*d*) yields the corresponding Bernoulli constant:

$$\bar{R}(s) = 2\gamma h(s) + [u'(h(s); s)]^2. \tag{2.4}$$

If $s < 0$, then the laminar flow defined by (2.3*a*,*b*) has a near-bottom counter-current, whereas the corresponding flow is unidirectional when $s > 0$. In what follows we assume that $s < 0$.

2.1. *Flattening transformation*

Changing the coordinates $(\bar{x}, \bar{y})$ to

$$(x, y) = \left(\bar{x}, \frac{\bar{y}}{\bar{\eta}(\bar{x})} h(s)\right), \tag{2.5}$$

we map the water domain onto the strip $\mathbb{R} \times (0, h(s))$. Let

$$\hat{\Phi}(x, y) = \bar{\psi}(\bar{x}, \bar{y}) \tag{2.6}$$

be a new unknown function, for which problem (2.2) with $\bar{R} = \bar{R}(s)$ takes the form

$$\left[\hat{\Phi}_x - \frac{y\bar{\eta}_x}{\bar{\eta}}\hat{\Phi}_y\right]_x - \frac{y\bar{\eta}_x}{\bar{\eta}}\left[\hat{\Phi}_x - \frac{y\bar{\eta}_x}{\bar{\eta}}\hat{\Phi}_y\right]_y + \frac{h^2(s)}{\bar{\eta}^2}\hat{\Phi}_{yy} - 1 = 0 \quad \text{for } 0 < y < h(s), \tag{2.7a}$$

$$\hat{\Phi}(x, 0) = 0 \quad \text{for } x \in \mathbb{R}, \tag{2.7b}$$

$$\hat{\Phi}(x, h(s)) = 1 \quad \text{for } x \in \mathbb{R}, \tag{2.7c}$$

$$\hat{\Phi}_y^2(x, h(s)) - \frac{\bar{\eta}^2(\bar{R}(s) - 2\gamma\bar{\eta})}{h(s)^2(1 + \bar{\eta}_x^2)} = 0 \quad \text{for } x \in \mathbb{R}. \tag{2.7d}$$

Note that $\hat{\Phi} = u(y; s)$ and $\bar{\eta} = h(s)$ is a solution of this system. Let us write (2.7) as a first-order system, for which purpose it is convenient to introduce the variable $\hat{\Psi}$ conjugate to $\hat{\Phi}$ (cf. Kozlov & Kuznetsov 2013):

$$\hat{\Psi}(x, y) = \frac{\bar{\eta}}{h(s)}\left[\hat{\Phi}_x - \frac{y\bar{\eta}_x}{\bar{\eta}}\hat{\Phi}_y\right]. \tag{2.8}$$

This allows us to write (2.7) as follows:

$$\hat{\Phi}_x = \frac{h(s)}{\bar{\eta}}\hat{\Psi} + \frac{y}{\bar{\eta}}\bar{\eta}_x\hat{\Phi}_y \quad \text{for } (x, y) \in \mathbb{R} \times (0, h(s)), \tag{2.9a}$$

$$\hat{\Psi}_x = \frac{\bar{\eta}_x}{\bar{\eta}}(y\hat{\Psi})_y - \frac{h(s)}{\bar{\eta}}\hat{\Phi}_{yy} + \frac{\bar{\eta}}{h(s)} \quad \text{for } (x, y) \in \mathbb{R} \times (0, h(s)), \tag{2.9b}$$

$$\hat{\Phi}(x, 0) = \hat{\Psi}(x, 0) = 0 \quad \text{for } x \in \mathbb{R}, \tag{2.9c}$$

$$\hat{\Phi}(x, y) = 1 \quad \text{on } y = h(s), \tag{2.9d}$$

$$\hat{\Phi}_y^2 + \hat{\Psi}^2 = \frac{\bar{\eta}^2}{h^2(s)}(\bar{R}(s) - 2\gamma\bar{\eta}) \quad \text{on } y = h(s). \tag{2.9e}$$

Furthermore, we have that

$$\bar{\eta}_x(x) = -\frac{\hat{\Psi}(x, h(s))}{\hat{\Phi}_y(x, h(s))}. \tag{2.10}$$

Relations (2.9) can be considered as an infinite-dimensional dynamical system for $\hat{\Phi}$ and $\hat{\Psi}$ only. Indeed, $\bar{\eta}$ and $\bar{\eta}_x$ can be eliminated with the help of (2.9*e*) and (2.10), which will be formalized in the next section.

2.2. *Linearization around a laminar flow*

Let us linearize relations (2.9) around the stream solution $\hat{\Phi} = u(y; s)$, $\hat{\Psi} = 0$, $\bar{\eta} = h(s)$, for which purpose we introduce

$$\Phi = \hat{\Phi} - u - \frac{yu_y}{h(s)}\zeta, \quad \Psi = \hat{\Psi}, \quad \zeta = \bar{\eta} - h(s). \tag{2.11a–c}$$

Then we obtain from (2.9):

$$\Phi_x = \Psi + N_1 \quad \text{for } (x, y) \in \mathbb{R} \times (0, h(s)), \tag{2.12a}$$

$$\Psi_x = -\Phi_{yy} + N_2 \quad \text{for } (x, y) \in \mathbb{R} \times (0, h(s)), \tag{2.12b}$$

$$\Phi(x, 0) = \Psi(x, 0) = 0 \quad \text{for } x \in \mathbb{R}, \tag{2.12c}$$

$$\Phi_y - \kappa\Phi = N_3 \quad \text{on } y = h(s). \tag{2.12d}$$

Here

$$\kappa = \kappa(s, \gamma) = \frac{\gamma + k}{k^2} \quad \text{and} \quad k = k(s) = h(s) + s = \sqrt{2 + s^2} > 0, \tag{2.13a,b}$$

whereas the nonlinear operators in (2.12*a*), (2.12*b*) and (2.12*c*) have the form

$$\left.\begin{aligned} N_1 &= \frac{-h(s)\Psi\zeta + y\zeta_x(y\zeta + h(s)\Phi_y)}{h(s)(h(s) + \zeta)}, \\ N_2 &= \frac{\zeta^2 + h(s)\zeta_x(y\Psi)_y + h(s)\zeta\Phi_{yy}}{h(s)(h(s) + \zeta)}, \\ N_3 &= \frac{-h(s)^2\Psi^2 + (\zeta + \Phi_y)(-h(s)\zeta(h(s) - 2k) + 2\zeta^2 k - h(s)^2\Phi_y)}{2(h(s) + \zeta)^2 k}, \end{aligned}\right\} \tag{2.14}$$

respectively. Moreover, we find that

$$\zeta(x) = -\frac{\Phi(x, h(s))}{k}, \quad \zeta_x(x) = -\frac{h(s)\Psi(x, h(s))}{h(s)\zeta + h(s)k + \zeta k + h(s)\Phi_y(x, h(s))}. \tag{2.15a,b}$$

Substituting these expressions into formulae for N_1, N_2 and N_3, we see that (2.12*a*) and (2.12*b*) form an infinite-dimensional reversible dynamical system on the manifold defined by (2.12*c*) and (2.12*d*); the mapping $(\Phi, \Psi) \mapsto (\Phi, -\Psi)$ is the reverser. Nonlinearity of the boundary condition (2.12*d*) is inessential in view of its reducibility to a homogeneous one by a proper change of variables; see Groves & Wahlén (2008) and Kozlov & Lokharu (2019) for details.

Let us assume that $\Psi \in C(\mathbb{R}; X_1)$ and $\Phi \in C(\mathbb{R}; X_2)$, where $X_m = \{f \in H^m(0, 1) : f(0) = 0\}$, $m = 1, 2$, and $H^m(0, 1)$ stands for the corresponding Sobolev space. Since k and κ depend analytically on s and γ belonging to a small neighbourhood of the origin, the same is true for the operators N_1, N_2 and N_3. More precisely, let

$$\Lambda_\epsilon = \{\lambda = (s, \gamma) \in \mathbb{R}^2 : |s|^2 + |\gamma|^2 < \epsilon^2\} \tag{2.16}$$

be a small neighbourhood of the origin in the parameter space, then

$$N_1 \in C^\infty(X_1 \times X_2 \times \Lambda_\epsilon; H^1(0, 1)), \quad N_2 \in C^\infty(X_1 \times X_2 \times \Lambda_\epsilon; L^2(0, 1)), \tag{2.17a,b}$$

whereas $N_3 \in C^\infty(X_1 \times X_2 \times \Lambda_\epsilon; \mathbb{R})$. Moreover, all derivatives of these operators are bounded and uniformly continuous in Λ_ϵ.

2.3. *A linear eigenvalue problem*

The centre subspace of system (2.12) is determined by the imaginary spectrum of the linear operator $\mathcal{L}(\Psi, \Phi) = (-\Phi_{yy}, \Psi)$ defined on a subspace of $X_1 \times X_2$ and subject to the homogeneous condition

$$\Phi_y(h(s)) = \kappa\Phi(h(s)). \tag{2.18}$$

It is straightforward to establish that the spectrum of $\mathcal{L}$ is discrete and consists of all $\hat{\tau} \in \mathbb{C}$ such that $\mu = \hat{\tau}^2$ is an eigenvalue of the following Sturm–Liouville problem:

$$-\varphi_{yy} = \mu\varphi \quad \text{on } (0, h(s)); \quad \varphi(0) = 0 \quad \text{and} \quad [\varphi_y - \kappa\varphi]_{y=h(s)} = 0. \tag{2.19a,b}$$

(Basic facts about Sturm–Liouville problems can be found in Teschl (2012).) Thus, the imaginary spectrum of $\mathcal{L}$ corresponds to the negative eigenvalues of (2.19*a*,*b*).

The spectrum of (2.19*a*,*b*) is discrete and consists of real simple eigenvalues, say

$$\mu_1 < \mu_2 < \cdots < \mu_j < \cdots, \tag{2.20}$$

accumulating at infinity, whereas the corresponding eigenfunctions φ_j can be rescaled to form an orthonormal basis in $L^2(0, h(s))$.

2.4. *On the existence of a negative eigenvalue*

Let us investigate the spectral problem (2.19*a*,*b*) for negative s and positive γ such that $\lambda = (s, \gamma) \in \Lambda_\epsilon$ and ϵ is sufficiently small. Solving (2.19*a*,*b*) explicitly, we find that μ_1 is

the unique negative eigenvalue equal to, say $-\tau^2$, provided τ is defined by the dispersion equation:

$$\tau h(s)\coth(\tau h(s)) = \kappa h(s). \tag{2.21}$$

Using the definition of κ, we see that

$$\kappa h(s) = 1 + \frac{\gamma - s}{\sqrt{2}} + O(s^2) \quad \text{as } s \to 0. \tag{2.22}$$

Therefore, $\kappa h(s) > 1$ for all $s < 0$ and $\gamma > 0$ such that $(s, \gamma) \in \Lambda_\epsilon$, and so the dispersion equation has a unique root $\tau > 0$ such that

$$[\tau h(s)]^2 = 3\frac{\gamma - s}{\sqrt{2}} + O(|s|^2 + |\gamma|^2) \quad \text{as } s, \gamma \to 0. \tag{2.23}$$

Since $[h(s)]^2 = 2 + O(s)$ as $s \to 0$, we see that τ tends to zero as $s, \gamma \to 0$. Therefore, some asymptotic formulae below will be written in terms of the small parameter τ. Let us summarize.

If $\gamma - s$ is positive, which is the case when $s < 0$, then (2.19*a*,*b*) has a negative eigenvalue $\mu_1 = -\tau^2$. Moreover, there exists only one such eigenvalue and $\tau \to 0$ as $s, \gamma \to 0$; the corresponding normalized eigenfunction has the asymptotic formula

$$\varphi_1(y) = c_0 y[1 + O(|s|^2 + |\gamma|^2)] \quad \text{as } s, \gamma \to 0, \text{ where } c_0 = \sqrt{\frac{3}{2^{3/2}}}, \tag{2.24}$$

and (2.24) is uniform with respect to $y \in [0, h(s)]$ and $\lambda = (s, \gamma) \in \Lambda_\epsilon$. The positive spectrum of $\mathcal{L}$ is separated from zero, because $\mu_2 > \pi^2/h^2(s) > \pi^2/2$ for small negative s.

3. Reduction to a finite-dimensional system

Let us reduce system (2.12) to a finite-dimensional Hamiltonian one, for which purpose the centre-manifold technique of Mielke (1988) (he considered quasilinear elliptic problems in cylinders) is used. For this purpose we apply a result obtained by Kozlov & Lokharu (2019); namely, their theorem 3.1 provides a convenient way for obtaining a reduced problem. Prior to that, the so-called spectral splitting is applied to decompose the system.

3.1. *Spectral decomposition and reduction*

Following the method proposed by Kozlov & Lokharu (2019), we seek (Φ, Ψ) in the form

$$\Phi(x, y) = \alpha(x)\varphi_1(y) + \widetilde{\Phi}(x, y), \quad \Psi(x, y) = \beta(x)\varphi_1(y) + \widetilde{\Psi}(x, y), \tag{3.1a,b}$$

where $\tilde{\Phi}$ and $\tilde{\Psi}$ are orthogonal to φ_1 in $L^2(0, h(s))$; that is,

$$\alpha(x) = \int_0^{h(s)} \Phi(x, y)\varphi_1(y)\,\mathrm{d}y, \quad \beta(x) = \int_0^{h(s)} \Psi(x, y)\varphi_1(y)\,\mathrm{d}y. \tag{3.2a,b}$$

For $\lambda \in \Lambda_\epsilon$ we define projectors $\mathcal{P}_\lambda\phi = \alpha\varphi_1$ and $\tilde{\mathcal{P}}_\lambda = \mathrm{id} - \mathcal{P}_\lambda$, which are well defined on $H^1(0, h(s))$ and orthogonal in $L^2(0, h(s))$. Multiplying (2.12*a*) and (2.12*b*) by φ_1 and

integrating over $(0, h(s))$, we obtain

$$\alpha_X = \beta + F_1(\Psi, \Phi; \lambda), \tag{3.3}$$

$$\beta_X = -\tau^2\alpha + F_2(\Psi, \Phi; \lambda), \tag{3.4}$$

where

$$\left.\begin{aligned} F_1(\Psi, \Phi; \lambda) &= \int_0^{h(s)} N_1(\Psi, \Phi; \lambda)\varphi_1 \,\mathrm{d}y, \\ F_2(\Psi, \Phi; \lambda) &= \int_0^{h(s)} N_2(\Psi, \Phi; \lambda)\varphi_1 \,\mathrm{d}y - N_3(\Psi, \Phi; \lambda)\varphi_1(h(s)). \end{aligned}\right\} \tag{3.5}$$

The system for $\tilde{\Phi}$ and $\tilde{\Psi}$ is as follows:

$$\tilde{\Phi}_x = \tilde{\Psi} + \tilde{\mathcal{P}}_\lambda(N_1), \tag{3.6}$$

$$\tilde{\Psi}_x = -\tilde{\Phi}_{yy} + \tilde{\mathcal{P}}_\lambda(N_2) + \varphi_1(h(s))\varphi_1 N_3, \tag{3.7}$$

and these functions satisfy the following boundary conditions:

$$\tilde{\Phi}(x, 0) = \tilde{\Psi}(x, 0) = 0, \quad \tilde{\Phi}_Y(x, h(s)) - \kappa\,\tilde{\Phi}(x, h(s)) = N_3. \tag{3.8a,b}$$

Let $\tilde{X}_j^{(\lambda)}$ denote $\tilde{\mathcal{P}}_\lambda(X_j)$, $j = 0, 1, 2$, where $\lambda \in \Lambda_\epsilon$, and so $\tilde{\Psi} \in \tilde{X}_1^{(\lambda)}$ and $\tilde{\Phi} \in \tilde{X}_2^{(\lambda)}$ for all $x \in \mathbb{R}$ and $\lambda \in \Lambda_\epsilon$. Then theorem 3.1 proved in Kozlov & Lokharu (2019) yields the following assertion for the decomposed system (3.3)–(3.8a,b).

THEOREM 3.1. *For any $m \geq 2$ there exist $\epsilon > 0$, neighbourhoods $W \subset \mathbb{R}^2$, $W_1 \subset X_1$, $W_2 \subset X_2$ and the vector-functions $r_j : W \times \Lambda_\epsilon \to W_j$, $j = 1, 2$, of the class $C^m(W \times \Lambda_\epsilon)$ with the following properties.*

(i) The derivatives of r_1 and r_2 are bounded and uniformly continuous, and the estimate

$$\|r_1; H^1\| + \|r_2; H^2\| = O(|\alpha|^2 + |\beta|^2), \quad \text{where } (\alpha, \beta) \in W, \tag{3.9}$$

holds uniformly with respect to $\lambda \in \Lambda_\epsilon$.

(ii) $r_j(\alpha, \beta, \lambda) \in \tilde{X}_j^{(\lambda)}$, $j = 1, 2$, for all $\lambda \in \Lambda_\epsilon$ and all $(\alpha, \beta) \in W$.

(iii) The set $M^\lambda = \{(\Psi^r[\alpha, \beta; \lambda], \Phi^r[\alpha, \beta; \lambda]) : (\alpha, \beta) \in W,\ \lambda \in \Lambda_\epsilon\} \subset X_1 \times X_2$, where

$$\Psi^r[\alpha, \beta; \lambda] = \beta\varphi_1 + r_1(\alpha, \beta; \lambda) \quad \text{and} \quad \Phi^r[\alpha, \beta; \lambda] = \alpha\varphi_1 + r_2(\alpha, \beta; \lambda), \tag{3.10}$$

is a locally invariant manifold for (2.12), that is, through every point of M^λ goes only one solution of (2.12) and it belongs to M^λ as long as $(r_1, r_2) \in W_1 \times W_2$.

(iv) Every global solution $(\alpha, \beta) \in C(\mathbb{R}; W)$ of the reduced system

$$\left.\begin{aligned} \alpha_x &= \beta + F_1(\Psi^r[\alpha, \beta; \lambda], \Phi^r[\alpha, \beta; \lambda]; \lambda), \\ \beta_x &= \mu_1\alpha + F_2(\Psi^r[\alpha, \beta; \lambda], \Phi^r[\alpha, \beta; \lambda]; \lambda), \end{aligned}\right\} \tag{3.11}$$

where $\lambda \in \Lambda_\epsilon$, generates the solution (Ψ, Φ) of (2.12) with

$$\Psi(x, y) = \Psi^r[\alpha(x), \beta(x); \lambda](y), \quad \Phi(x, y) = \Phi^r[\alpha(x), \beta(x); \lambda](y). \tag{3.12a,b}$$

Moreover, the reduced system (3.11) is reversible.

A direct calculation shows that the reduced system (3.11) has the following structure:

$$\begin{aligned}\alpha_x &= \beta[1 + O(|\alpha| + |\alpha|^2 + |\beta|^2)],\\ \beta_x &= -\tau^2\alpha + A\alpha^2 + O(|\alpha|^3 + |\beta|^2),\end{aligned} \tag{3.13}$$

where $A = \frac{1}{2}c_0^3 + O(|s|^2 + |\gamma|^2)$ as $s, \gamma \to 0$ and c_0 is the constant defined in (2.24); hence $A = \sqrt{3^3/2^{13/2}} + O(|s|^2 + |\gamma|^2)$. Now, we are in a position to formulate and prove the following.

THEOREM 3.2. *Problem (3.13) has a homoclinic solution such that*

$$\alpha_h(x) = \tau^2\alpha_+^\star - \left[\tfrac{3}{2}\alpha_+^\star\tau^2 + O(\tau^4)\right] sech^2(\tau x/2) \quad as\ \tau \to 0, \tag{3.14}$$

whereas β_h is defined implicitly by the first formula (3.13). Here $\alpha_+^\star = A^{-1} + O(\tau^2)$ is a constant independent of x.

Proof. It is known (see Groves & Stylianou 2014; Kozlov & Kuznetsov 2013) that problem (1.1*a*)–(1.1*d*) has a Hamiltonian structure (even for arbitrary vorticity) with the horizontal coordinate playing the role of time. The corresponding Hamiltonian is the flow force invariant; in the original coordinates (X, Y), it has the following form:

$$\mathcal{S} = \left[\tfrac{1}{2}R - b\right]\eta(X) - \tfrac{1}{2}\left\{\eta^2(X) - \int_0^{\eta(X)} \tfrac{1}{2}(\psi_Y^2 - \psi_X^2) + b\psi\, \mathrm{d}Y\right\}. \tag{3.15}$$

Thus, the reduced system (3.13) has a constant of motion $\mathcal{H}(\alpha, \beta)$; to obtain an expression for it one has to subject $b^{-1}\mathcal{S}$ to all changes of variables described above. A direct calculation yields that

$$\mathcal{H}(\alpha, \beta) = \frac{1}{2}\left(\beta^2 + \tau^2\alpha^2\right) - \frac{A}{3}\alpha^3 + O\left(\alpha^4 + \beta^2\right) (= b^{-1}S), \tag{3.16}$$

where A is the coefficient in the second equation (3.13). It should be noted that $\mathcal{H}(\alpha, \beta)$ is an even function of β which follows from reversibility of this system. The form of $\mathcal{H}(\alpha, \beta)$ suggests that variables must be scaled as follows:

$$\alpha(x) = \tau^2\alpha_1(x_1), \quad \beta(x) = \tau^3\beta_1(x_1), \quad x = \tau^{-1}x_1, \quad \mathcal{H}(\alpha, \beta) = \tau^6\mathcal{H}_1(\alpha_1, \beta_1), \tag{3.17a–d}$$

where

$$\mathcal{H}_1(\alpha_1, \beta_1) = \frac{1}{2}\left(\alpha_1^2 + \beta_1^2\right) - \frac{A}{3}\alpha_1^3 + \tau^2 O\left(|\alpha_1^3| + |\beta_1^4|\right), \tag{3.18}$$

and so the scaled equations are

$$\begin{aligned}[\alpha_1]_{x_1} &= \beta_1 + \tau^2\beta_1 O\left(|\alpha_1| + |\beta_1|^2\right),\\ [\beta_1]_{x_1} &= -\alpha_1 + A\alpha_1^2 + \tau^2 O\left(|\alpha_1|^3 + |\beta_1|^2\right).\end{aligned} \tag{3.19}$$

The graph of $\mathcal{H}_1(\alpha, 0)$ in a neighbourhood of the origin is sketched in figure 3(*a*). It is clear that the local maximum of this function close to the origin is attained at $\alpha = \alpha_+^\star$ and

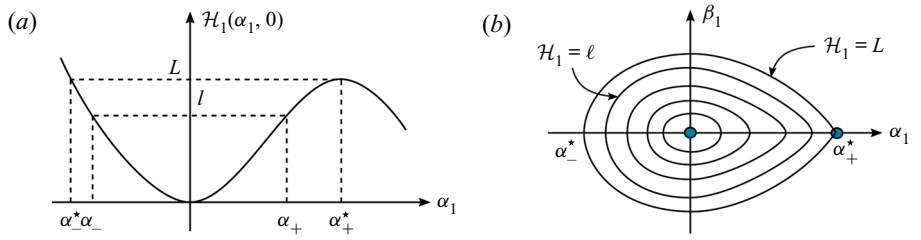

FIGURE 3. The behaviour of the Hamiltonian near the origin (*a*) and its level curves (*b*). (*a*) Graph of the function $\mathcal{H}_1(\alpha_1, 0)$. (*b*) Phase portrait.

$L = \mathcal{H}_1(\alpha_+^\star, 0)$ is its value. Then the level line

$$\mathcal{H}_1(\alpha_1, \beta_1) = \ell \tag{3.20}$$

is a closed curve for every $\ell \in (0, L)$ and it corresponds to a periodic solution. The contour

$$\mathcal{H}_1(\alpha_1, \beta_1) = L \tag{3.21}$$

defines the homoclinic orbit; see a sketch of level lines in figure 3(*b*). The values $\alpha_-^\star$ and $\alpha_+^\star$ correspond to the 'crest' level and the limiting depth, respectively. An essential feature of the homoclinic orbit is that α_1 attains negative values on its left-hand part; this implies that there is a stagnation point as will be shown below.

Let us turn to proving (3.14). By α_1^h we denote a homoclinic solution to (3.19). It is easy to see that it is monotone on each side of the crest which corresponds to the value $\alpha_1^h(0) = \alpha_-^\star$. Then we have

$$X_1 = \int_0^{x_1} \mathrm{d}x_1 = \int_{\alpha_-^\star}^{\alpha_1^h(x_1)} \frac{\mathrm{d}\alpha_1}{[\alpha_1^h]_{x_1}}, \tag{3.22}$$

where $[\alpha_1^h]_{x_1} = \beta_1^h[1 + O(\tau^2)]$; see the first equation (3.19). On the other hand,

$$L - \mathcal{H}_1(\alpha_1^h, 0) = \frac{[\beta_1^h]^2}{2}\left\{1 + \tau^2 O([\beta_1^h]^2)\right\}, \tag{3.23}$$

where the system's reversibility is used. Expressing $[\beta_1^h]^2$ from the last formula and taking into account the fact that it is positive on the interval of the integration, we obtain

$$x_1 = \int_{\alpha_-^\star}^{\alpha_1^h(x_1)} \frac{\mathrm{d}\alpha_1}{[\alpha_1^h]_{x_1}} = [1 + O(\tau^2)] \int_{\alpha_-^\star}^{\alpha_1^h(x_1)} \frac{\mathrm{d}\alpha_1}{\sqrt{2[L - \mathcal{H}_1(\alpha_1^h, 0)]}}. \tag{3.24}$$

Let us find an approximation of the integral using a third-degree polynomial for the expression under the square root; more precisely, let us show that

$$L - \mathcal{H}_1(\alpha_1, 0) = a(\tau)(\alpha_1 - \alpha_-^\star)(\alpha_1 - \alpha_+^\star)^2 + \tau^2 O(|\alpha_1 - \alpha_-^\star||\alpha_1 - \alpha_+^\star|^2), \tag{3.25}$$

where

$$a(\tau) = -\frac{L}{\alpha_-^\star[\alpha_+^\star]^2} = \frac{A}{3} + O(\tau^2). \tag{3.26}$$

It should be emphasized that (3.25) is used as a representation of $L-\mathcal{H}_1(\alpha_1,0)$ only on the interval $[\alpha_-^\star,\alpha_+^\star]$. To prove (3.25) we note that

$$L-\mathcal{H}_1(\alpha_1,0)=L-\frac{\alpha_1^2}{2}+A\frac{\alpha_1^3}{3}+\tau^2O(|\alpha_1|^3)=:Q_1(\alpha_1)+\tau^2O(|\alpha_1|^3). \tag{3.27}$$

A direct calculation yields that the estimate $O(\tau^2)$ holds for

$$Q_1(\alpha_-^\star),\quad Q_1(\alpha_+^\star),\quad \partial_{\alpha_1}Q_1(\alpha_+^\star). \tag{3.28a–c}$$

Therefore, solving a linear system, one obtains that up to $O(\tau^2)$ the coefficients of

$$a(\tau)(\alpha_1-\alpha_-^\star)(\alpha_1-\alpha_+^\star)^2 \tag{3.29}$$

are the same as those of Q_1. This shows that the error in (3.25) has the same estimate $O(\tau^2)$. It remains to use the fact that $L-\mathcal{H}_1(\alpha_1,0)$ has a simple zero at $\alpha_-^\star$ and a double zero at $\alpha_+^\star$ which proves (3.25).

Now we have

$$\begin{aligned}\int_{\alpha_-^\star}^{\alpha_1^h(x_1)}\frac{\mathrm{d}\alpha_1}{\sqrt{2(L-\mathcal{H}_1(\alpha_1,0))}}&=[1+O(\tau^2)]\int_{\alpha_-^\star}^{\alpha_1^h(x_1)}\frac{\mathrm{d}\alpha_1}{\sqrt{2a(\alpha_1-\alpha_-^\star)(\alpha_1-\alpha_+^\star)^2}}\\&=\frac{1+O(\tau^2)}{a_0\sqrt{2a}}\left[\ln\left|\frac{a_0+\sqrt{\alpha_1-\alpha_-^\star}}{a_0-\sqrt{\alpha_1-\alpha_-^\star}}\right|\right]_{\alpha_1=\alpha_-^\star}^{\alpha_1=\alpha_1^h(x_1)}\\&=\frac{1+O(\tau^2)}{a_0\sqrt{2a}}\left(\ln\left[\frac{\left(a_0+\sqrt{\alpha_1^h(x_1)-\alpha_-^\star}\right)^2}{\alpha_+^\star-\alpha_1^h(x_1)}\right]\right),\end{aligned} \tag{3.30}$$

where $a_0=\sqrt{\alpha_+^\star-\alpha_-^\star}$. Comparing this and (3.24), one obtains the following asymptotic formula for the solitary-wave solution:

$$\alpha_1^h(x_1)=\alpha_+^\star-\left[\frac{6}{A}+O(\tau^2)\right]\mathrm{e}(-(1+O(\tau^2))x_1)\quad\text{as }\tau\to0, \tag{3.31}$$

where the formulae $\alpha_-^\star=-\alpha_+^\star/2+O(\tau^2)$ and $\alpha_+^\star=A^{-1}+O(\tau^2)$ are taken into account. Furthermore, it is straightforward to show that

$$\|\alpha_1^h-\alpha_1^{h,\star}\|_{L^\infty(\mathbb{R})}=O(\tau^2)\quad\text{as }\tau\to0, \tag{3.32}$$

where

$$\alpha_1^{h,\star}(x_1)=\frac{1}{A}-\frac{3}{2A}\operatorname{sech}^2(x_1/2). \tag{3.33}$$

The latter is a homoclinic solution of (3.19) with $\tau=0$, in which case $\beta_1=[\alpha_1^{h,\star}]_{x_1}$. Combining this and the asymptotic formula (3.31), one arrives at (3.14) by rescaling variables to the original ones. □

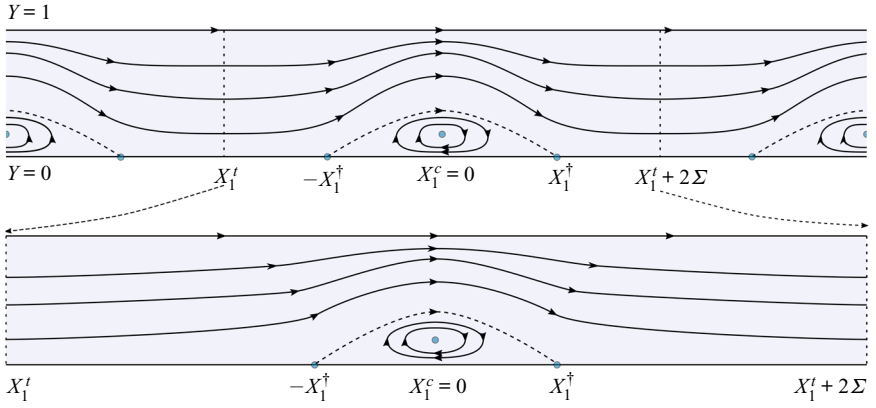

FIGURE 4. Two Stokes waves corresponding to different values of ℓ plotted in (X_1, Y) variables.

3.2. *Periodic waves*

The streamline pattern for periodic solutions was studied in Wahlén (2009). It was shown that below every crest there is a cat's-eye region adjacent to the bottom as in figure 4. Our aim is to show that this region stays bounded as $\ell \to L$, so that the solitary wave has a similar streamline pattern.

An approximation of solutions for periodic waves can be found in the same way as for solitary waves. Indeed, let us consider the periodic solution α_1^ℓ corresponding to some energy $\mathcal{H}_1 = \ell$. Let a trough of this wave be located at $x_1^c = 0$ and let the nearest crest to the left be at $x_1^t < x_1^c$ (see figure 4). Then for every $x_1 \in (x_1^t x_1^c]$ we have

$$x_1 - x_1^t = \int_{\alpha_-}^{\alpha_1^\ell(x_1)} \frac{\mathrm{d}\alpha_1}{[\alpha_1^\ell]_{x_1}} = [1 + O(\tau^2)] \int_{\alpha_-}^{\alpha_1^\ell(x_1)} \frac{\mathrm{d}\alpha_1}{\sqrt{2[\ell - \mathcal{H}_1(\alpha_1, 0)]}}. \tag{3.34}$$

In particular, the half-period of this solution is equal to

$$\Sigma_\ell = x_1^c - x_1^t = [1 + O(\tau^2)] \int_{\alpha_-}^{\alpha_+} \frac{\mathrm{d}\alpha_1}{\sqrt{2[\ell - \mathcal{H}_1(\alpha_1, 0)]}}, \tag{3.35}$$

and so $\Sigma_\ell \to +\infty$ as $\ell \to L$. Let us estimate the bottom width of a cat's-eye vortex (in figure 4, it is bounded above by the dashed streamline). On every interval symmetric about the crest and having the length $2\Sigma_\ell$, there are exactly two stagnation points on the bottom that bound the bottom-attached vortex (these points are plotted as dots in figure 4), and $\alpha_1^\ell(\pm x_1^\dagger) = 0$ at these points nearest to the origin. From (3.34) the approximate formula follows:

$$-x_1^\dagger - x_1^t = [1 + O(\tau^2)] \int_{\alpha_-}^{0} \frac{\mathrm{d}\alpha_1}{\sqrt{2[\ell - \mathcal{H}_1(\alpha_1, 0)]}}, \tag{3.36}$$

which yields that $x_1^\dagger = O(1)$ as $\ell \to L$ in view that the integral

$$\int_{\alpha_-}^{0} \frac{\mathrm{d}\alpha_1}{\sqrt{2[L - \mathcal{H}_1(\alpha_1, 0)]}} \tag{3.37}$$

is finite. Indeed, the function $L - \mathcal{H}_1(\alpha_1, 0)$ has only one simple zero $\alpha_1 = \alpha_-^\star$ on the interval of integration. Thus, $x_1^\dagger$ remains bounded when the wavelength goes to infinity,

and the same is true for the domain occupied by cat's-eye vortex. Therefore, the pattern of streamlines remains the same for the limiting solitary wave (see figure 1).

4. Proof of theorem 1.1

From (3.31), it is straightforward to recover the asymptotics of the free-surface profile in the original non-dimensional coordinates; it looks as follows:

$$\eta(X) = h_- + \sqrt{b}\left[\frac{3}{c_0^2} + O(\tau^2)\right]\tau^2\mathrm{sech}^2(\sqrt{b}\tau X/2) \quad \text{as } \tau \to 0, \tag{4.1}$$

and so describes a solitary wave of elevation. Here, the depth at infinity is $h_- = h(s) + 2s$, which coincides with that of the unidirectional laminar flow conjugate to (2.3*a*,*b*). (Thus, this flow supports solitary waves similarly to the irrotational case.) Furthermore, c_0 is the constant defined in (2.24) and τ is the unique positive root of the dispersion equation (2.21), which, according to (2.23), tends to zero as $s \to 0$ and $b \to \infty$ simultaneously (indeed, $\gamma = b^{-3/2}$).

To show that the flow supporting this wave has a bottom-attached cat's-eye vortex, let us track back the changes of coordinates made above and find that

$$\hat{\Phi}_y = u_y + \Phi_y - (u_y + y)\Phi(x, h)/(kh). \tag{4.2}$$

Here $\Phi(x, y) = \alpha(x)\varphi_1(y) + yO(\tau^4) = c_0 y[\alpha(x) + O(\tau^4)]$ as $\tau \to 0$, where the second equality is a consequence of (2.24). Hence we see that

$$\begin{aligned}\hat{\Phi}_y = u_y\left[1 - \frac{c_0\alpha(x)}{\sqrt{2+s^2}} + O(|s|^2 + |\gamma|^2) + O(y)\right]\\ + \alpha(x)[c_0 + O(y)] \quad \text{as } s, \gamma \to 0 \text{ and } y \to 0.\end{aligned} \tag{4.3}$$

The first term is negative near the bottom because $u_y < 0$ according to formula (2.3*a*,*b*) and the assumption that $s < 0$, whereas the expression in the square brackets is positive. Moreover, it was established in the proof of theorem 3.2 that $\alpha(x)$ is negative on some interval. Taking this into account, the second term in the last formula also attains negative values near the bottom which shows that the same is true for $\hat{\Phi}_y$.

It follows from considerations in § 3.2 that the cat's-eye region shown in figure 4 remains bounded as $\ell \to L$. This yields that the pattern of streamlines of $\hat{\Phi}$ has the structure plotted in figure 1. Since the pattern of streamlines of ψ is essentially the same, this completes the proof of theorem 1.1.

5. Concluding remarks

We have considered the problem describing water waves in a rotational flow of finite depth when the corresponding unperturbed shear flow has a near-bottom counter-current. The latter flow exists, in particular, when the vorticity is a negative constant; its value is assumed to be large which simplifies the analysis as to whether this flow supports a solitary wave. It was emphasized by Benjamin (1962) that investigating propagation of waves, it is essential to avoid the artificial assumption of irrotational motion because it ignores the effects of friction and current. In the model presented here, the latter is taken into account directly by the vorticity distribution, whereas the former is treated as diffused over the whole cross-section of an infinitely long channel.

Our approach combines scaling and the spatial dynamics technique. By scaling, the problem is shown to be equivalent to another one, in which the vorticity is equal to -1, whereas the gravity constant $\gamma > 0$ is treated as a small parameter depending on the original vorticity. Moreover, an extra parameter is involved in our construction, namely the velocity $s < 0$ of the unperturbed flow at the bottom. The main results are that this flow supports a solitary wave provided γ and s are sufficiently small, whereas the pattern of streamlines contains a bottom-attached region below the crest, where they are closed and surround an interior stagnation point. This extends previous results on solitary waves concerning unidirectional flows only to the more complicated flow.

It occurs that the presence of two parameters even simplifies tackling the problem despite neither of them being suitable for use in the spatial dynamics method in the same way as in Groves & Wahlén (2008). Nevertheless, this method is applicable, because there is another natural small parameter. Indeed, the centre subspace of the spatial dynamics method is determined by the imaginary spectrum of the linearized operator defined by a nonlinear system. We linearize our system depending on the parameter γ (it arises after a flattening transformation which is a standard procedure when the partial hodograph transform cannot be used) around the stream solution involving the second parameter s and this leads to a Sturm–Liouville problem. If both γ and s are small, then it has only one negative eigenvalue, $-\tau^2$, where τ is a unique positive root of the dispersion equation. Moreover, $\tau \to 0$ as γ and s go to zero, and so it is convenient to use τ as a small parameter while analysing a finite-dimensional Hamiltonian system to which the original one reduces.

As in the simpler case studied by Groves & Wahlén (2008), there exists a homoclinic solution of the finite-dimensional system, and it is expressed in terms of the hyperbolic secant, but in a more complicated way. Moreover, the asymptotic formula (4.1) recovered from the homoclinic solution expresses the free-surface profile of a solitary wave in the original coordinates. Presumably, this formula is suitable for numerical computation of the profile. Indeed, if proper values of γ and s are taken, then the root τ can be found numerically from the dispersion equation (2.21) and used for evaluating (4.1). Computation of the corresponding streamlines is a more sophisticated task, as a paper by Ribeiro *et al.* (2017) dealing with periodic waves demonstrates. Adaptation of their method to solitary waves is a challenge to be investigated. Another question related to the latter paper is to find out whether the pressure on the bottom boundary is different from that in the irrotational case.

Acknowledgements

V.K. was supported by the Swedish Research Council (VR), 2017-03837. N.K. acknowledges support from Linköping University.

Declaration of interests

The authors report no conflict of interest.

REFERENCES

AASEN, A. & VARHOLM, K. 2017 Traveling gravity water waves with critical layers. *J. Math. Fluid Mech.* **20** (1), 161–187.

AMICK, C. J., FRAENKEL, L. E. & TOLAND, J. F. 1982 On the Stokes conjecture for the wave of extreme form. *Acta Mathematica* **148**, 193–214.

AMICK, C. J. & TOLAND, J. F. 1981*a* On periodic water-waves and their convergence to solitary waves in the long-wave limit. *Phil. Trans. R. Soc. Lond.* A **303** (1481), 633–669.

AMICK, C. J. & TOLAND, J. F. 1981*b* On solitary water-waves of finite amplitude. *Arch. Rat. Mech. Anal.* **76** (1), 9–95.

BENJAMIN, T. B. 1962 The solitary wave on a stream with an arbitrary distribution of vorticity. *J. Fluid Mech.* **12**, 97–116.

CONSTANTIN, A. 2010 On the particle paths in solitary water waves. *Q. Appl. Maths* **68** (1), 81–90.

CONSTANTIN, A. & ESCHER, J. 2007 Particle trajectories in solitary water waves. *Bull. Am. Math. Soc.* **44** (03), 423–432.

CONSTANTIN, A. & STRAUSS, W. 2004 Exact steady periodic water waves with vorticity. *Commun. Pure Appl. Maths* **57** (4), 481–527.

CONSTANTIN, A., STRAUSS, W. & VĂRVĂRUCĂ, E. 2016 Global bifurcation of steady gravity water waves with critical layers. *Acta Mathematica* **217** (2), 195–262.

CRAIG, W. & STERNBERG, P. 1988 Symmetry of solitary waves. *Commun. Part. Diff. Equ.* **13** (5), 603–633.

EHRNSTRÖM, M. 2008 A new formulation of the water wave problem for Stokes waves of constant vorticity. *J. Math. Anal. Appl.* **339**, 636–643.

EHRNSTRÖM, M., ESCHER, J. & WAHLÉN, E. 2011 Steady water waves with multiple critical layers. *SIAM J. Math. Anal.* **43** (3), 1436–1456.

FRIEDRICHS, K. O. & HYERS, D. H. 1954 The existence of solitary waves. *Commun. Pure Appl. Maths* **7**, 517–550.

GROVES, M. D. & NILSSON, D. V. 2018 Spatial dynamics methods for solitary waves on a ferrofluid jet. *J. Math. Fluid Mech.* **20**, 1427–1458.

GROVES, M. D. & STYLIANOU, A. 2014 On the Hamiltonian structure of the planar steady water-wave problem with vorticity. *C. R. Acad. Sci. Paris* **352** (3), 205–211.

GROVES, M. D. & WAHLÉN, E. 2007 Spatial dynamics methods for solitary gravity-capillary water waves with an arbitrary distribution of vorticity. *SIAM J. Math. Anal.* **39** (3), 932–964.

GROVES, M. D. & WAHLÉN, E. 2008 Small-amplitude Stokes and solitary gravity water waves with an arbitrary distribution of vorticity. *Physica* D **237** (10–12), 1530–1538.

HUR, V. M. 2008 Exact solitary water waves with vorticity. *Arch. Rat. Mech. Anal.* **188** (2), 213–244.

HUR, V. M. & WHEELER, M. H. 2020 Exact free surfaces in constant vorticity flows. *J. Fluid Mech.* **896**, R1.

KEADY, G. & NORBURY, J. 1978 On the existence theory for irrotational water waves. *Proc. Camb. Phil. Soc.* **83** (1), 137–157.

KIRCHGÄSSNER, K. 1982 Wave-solutions of reversible systems and applications. In *Dynamical Systems, II (Gainesville, Fla., 1981)*, pp. 181–200. Academic.

KIRCHGÄSSNER, K. 1988 Nonlinearly resonant surface waves and homoclinic bifurcation. In *Advances in Applied Mechanics*, vol. 26, pp. 135–181. Academic.

KOZLOV, V. & KUZNETSOV, N. 2013 Steady water waves with vorticity: spatial Hamiltonian structure. *J. Fluid Mech.* **733**, R1.

KOZLOV, V., KUZNETSOV, N. & LOKHARU, E. 2015 On bounds and non-existence in the problem of steady waves with vorticity. *J. Fluid Mech.* **765**, R1.

KOZLOV, V., KUZNETSOV, N. & LOKHARU, E. 2017 On the Benjamin–Lighthill conjecture for water waves with vorticity. *J. Fluid Mech.* **825**, 961–1001.

KOZLOV, V. & LOKHARU, E. 2017 N-modal steady water waves with vorticity. *J. Math. Fluid Mech.* **20** (2), 853–867.

KOZLOV, V. & LOKHARU, E. 2019 Small-amplitude steady water waves with critical layers: non-symmetric waves. *J. Diff. Equ.* **267** (7), 4170–4191.

LAVRENTIEV, M. A. 1954 On the theory of long waves. *Am. Math. Soc. Transl.* **102**, 3–50.

MAJDA, A. J. & BERTOZZI, A. L. 2002 *Vorticity and incompressible flow*. Cambridge Texts in Applied Mathematics, vol. 27. Cambridge University Press.

MCLEOD, J. B. 1984 The Froude number for solitary waves. *Proc. R. Soc. Edin.* **97**, 193–197.

MIELKE, A. 1986 A reduction principle for nonautonomous systems in infinite-dimensional spaces. *J. Diff. Equ.* **65** (1), 68–88.

MIELKE, A. 1988 Reduction of quasilinear elliptic equations in cylindrical domains with applications. *Math. Meth. Appl. Sci.* **10** (1), 51–66.

MIELKE, A. 1991 *Hamiltonian and Lagrangian Flows on Center Manifolds*. Springer.

RIBEIRO, R., MILEWSKI, P. A. & NACHBIN, A. 2017 Flow structure beneath rotational water waves with stagnation points. *J. Fluid Mech.* **812**, 792–814.

RUSSELL, J. S. 1844 Report on waves. In *Report of the fourteenth meeting of the British Association for the Advancement of Science, York*, pp. 311–390. John Murray.

SWAN, C., CUMMINGS, I. P. & JAMES, R. L. 2001 An experimental study of two-dimensional surface water waves propagating on depth-varying currents. *J. Fluid Mech.* **428**, 273–304.

TELES DA SILVA, A. F. & PEREGRINE, D. H. 1988 Steep, steady surface waves on water of finite depth with constant vorticity. *J. Fluid Mech.* **195**, 281–302.

TER-KRIKOROV, A. M. 1962 The solitary wave on the surface of a turbulent liquid. *USSR Comput. Math. Math. Phys.* **1** (4), 1253–1264.

TESCHL, G. 2012 *Ordinary differential equations and dynamical systems*. Graduate Studies in Mathematics, vol. 140. American Mathematical Society.

THOMAS, G. P. 1981 Wave-current interactions: an experimental and numerical study. Part 1. Linear waves. *J. Fluid Mech.* **110**, 457–474.

THOMAS, B. J. 1977 The existence of solitary water waves. *Commun. Pure. Appl. Maths* **30** (4), 373–389. https://onlinelibrary.wiley.com/doi/pdf/10.1002/cpa.3160300402.

VANDEN-BROECK, J.-M. 1994 Steep solitary waves in water of finite depth with constant vorticity. *J. Fluid Mech.* **274**, 339–348.

VANDEN-BROECK, J.-M. 1995 New families of steep solitary waves in water of finite depth with constant vorticity. *Eur. J. Mech. B/Fluids* **14**, 761–774.

VARVARUCA, E. 2008 Bernoulli free-boundary problems in strip-like domains and a property of permanent waves on water of finite depth. *Proc. R. Soc. Edin.* **138** (6), 1345–1362.

WAHLÉN, E. 2009 Steady water waves with a critical layer. *J. Diff. Equ.* **246** (6), 2468–2483.

WHEELER, M. H. 2013 Large-amplitude solitary water waves with vorticity. *SIAM J. Math. Anal.* **45** (5), 2937–2994.

WHEELER, M. H. 2015 The Froude number for solitary water waves with vorticity. *J. Fluid Mech.* **768**, 91–112.